Journal of Vacuum Science and Technology A

RESEARCH ARTICLE | MAY 02 2023

# Isotropic plasma-thermal atomic layer etching of aluminum nitride using $SF_6$ plasma and $Al(CH_3)_3$

Haozhe Wang ; Azmain Hossain ; David Catherall ; Austin J. Minnich



*J. Vac. Sci. Technol. A* 41, 032606 (2023)
https://doi.org/10.1116/6.0002476

JVST A
Journal of Vacuum Science & Technology A

ARTICLE

avs.scitation.org/journal/jva

# Isotropic plasma-thermal atomic layer etching of aluminum nitride using $SF_6$ plasma and $Al(CH_3)_3$

Cite as: J. Vac. Sci. Technol. A 41, 032606 (2023); doi: 10.1116/6.0002476
Submitted: 9 January 2023 · Accepted: 10 April 2023 ·
Published Online: 2 May 2023



Haozhe Wang, Azmain Hossain, David Catherall, and Austin J. Minnich[a]

AFFILIATIONS

Division of Engineering and Applied Science, California Institute of Technology, Pasadena, California 91125

[a]Author to whom correspondence should be addressed: aminnich@caltech.edu

## ABSTRACT

We report the isotropic plasma atomic layer etching (ALE) of aluminum nitride using sequential exposures of $SF_6$ plasma and trimethylaluminum [$Al(CH_3)_3$]. ALE was observed at temperatures greater than 200 °C, with a maximum etch rate of 1.9 Å/cycle observed at 300 °C as measured using *ex situ* ellipsometry. After ALE, the etched surface was found to contain a lower concentration of oxygen compared to the original surface and exhibited a ~ 35% decrease in surface roughness. These findings have relevance for applications of AlN in nonlinear photonics and wide bandgap semiconductor devices.





## I. INTRODUCTION

Aluminum nitride (AlN) is a III–V semiconductor of interest in photonics and electronics owing to its simultaneous strong second-order ($\chi^{(2)}$) and third-order ($\chi^{(3)}$) optical nonlinearities, wide bandgap (>6 eV), and high dielectric constant (~8.9).[1–3] AlN has the lowest optical loss among III–V group materials over a range of wavelengths from the ultraviolet to the mid-infrared[2,4] and is under investigation for applications in ultraviolet light emitting diodes[5,6] and optical quantum circuits.[7,8] High quality factors (* $10^6$) have been achieved in AlN microring resonators,[9,10] which are fundamental components of on-chip frequency combs and second-harmonic generation elements.[11–13] AlN also finds potential applications as a low-leakage gate dielectric[14–17] and has been employed in various thin film transistors.[18–20]

For these applications, limitations on figures of merit have been attributed to surface imperfections and microfabrication processes. For instance, the presence of a native oxide leads to unstable etch rates with dry etching processes.[21] The surface and sidewall roughness of etched nanostructures is on the order of 1 − 4 nm,[1,9,22] leading to light scattering. Poor-quality surface material with refractive index fluctuations may also lead to light scattering even on nominally smooth surfaces. These nonidealities result in waveguide loss and limit the quality factor of optical microresonators, which in turn affects the performance of on-chip photonic devices.[23]

Atomic layer etching (ALE) is an emerging subtractive nanofabrication process with the potential to address these limitations.[24–27] In isotropic ALE, a surface is etched using sequential reactions consisting of an initial surface modification followed by volatilization of the modified surface layer. Early development of ALE focused on directional etching using bombardment of a suitably prepared surface with low energy ions or neutral atoms.[28–30] Recently, isotropic ALE processes have been developed, which enable isotropic etching with angstrom-scale precision.[25] Thermal and plasma isotropic ALE recipes are now available for various dielectrics and semiconductors, including $Al_2O_3$,[31–36] $SiO_2$,[37,38] InGaAs,[39] and others.[25,40,41] Surface smoothing of etched surfaces using ALE has been reported for various materials, including $Al_2O_3$,[34,42] amorphous carbon,[43] and III–V semiconductors.[39,44] For AlN, isotropic ALE recipes have been reported using HF/Sn(acac)$_2$[45] and $XeF_2$ or HF and $BCl_3$,[46] yielding etch per cycle (EPC) of 0.36 and 0.93 Å/cycle, respectively. Exposure to $H_2$ plasma as a post-treatment in each cycle of the HF/Sn(acac)$_2$ recipe resulted in an increase in EPC to 1.96 Å/cycle. However, identifying alternate reactants to HF vapor and examining the potential for decreasing surface roughness remain of interest for ALE of AlN.

Here, we report the atomic layer etching of AlN using sequential exposures of $SF_6$ plasma and trimethylaluminum [$Al(CH_3)_3$, TMA], achieving up to 1.9 Å/cycle at 300 °C. The necessity of both half-reactions for etching was established by verifying that no etching occurred with only $SF_6$ plasma or TMA. The etched surface was characterized using atomic force microscopy and x-ray photoemission spectroscopy. The etched surface exhibited a decrease in roughness by ~35% over a range of spatial frequencies

after 50 cycles of ALE, and the ALE process was found to reduce the native oxide concentration at the surface. These improved surface characteristics highlight the potential of the process for applications in photonics and wide bandgap electronics.

## II. EXPERIMENT

The sequence for the plasma-assisted thermal ALE process is illustrated in Fig. 1(a). $SF_6$ plasma is first generated to fluorinate the surface using F radicals, producing $AlF_3$ on the AlN film surface. The excess gas phase reactants are then purged, and a TMA dose is introduced and held in the chamber. The TMA reacts with the $AlF_3$ in a ligand-exchange reaction, yielding volatile etching products.[47] We hypothesize that the surface chemical reactions are similar to those reported for the isotropic plasma ALE of alumina using the same reactants;[36] the specific reactions are a topic of future study.

This process was applied to AlN samples grown on Si (111) wafers by sputtering of an Al target gun with a flow of 10 sccm nitrogen and 20 sccm Ar. The initial AlN films had a thickness of 280 Å as measured by spectroscopic ellipsometry (J. A. Woolam) at 65°, 70°, and 75° from 370 to 1000 nm. The samples were 12 × 12 $mm^2$ chips. To determine the thickness change after a certain number of ALE cycles, nine points were measured using ellipsometry on each AlN sample using a preprogrammed 10 × 10 $mm^2$ square array with 5 mm spacing between points. Subsequently, the spectrum was fit by the Cauchy model to obtain the AlN thickness. The average thickness of a single sample was calculated using thicknesses measured and modeled by the nine points.

X-ray Photoemission Spectroscopy (XPS) analysis was performed using a Kratos Axis Ultra x-ray photoelectron spectrometer using a monochromatic Al $K\alpha$ source (Kratos Analytical). Depth profiling was performed using an Ar ion beam with a 60 s interval for each cycle. The total etch depth was measured by a Dektak XT Stylus profilometer. The estimated etch depth for each cycle was then obtained by assuming that the etching is uniform in all the cycles. The XPS data were analyzed in CASAXPS (Casa Software, Ltd.). As discussed in more detail below, the initial bulk composition of the films was found to be 55.9% (Al) 41.3% (N) 2.5% (O), values which are consistent with other studies.[48,49]

Isotropic plasma ALE was performed using a FlexAL atomic layer deposition system (Oxford Instruments). The sample was placed on a 6-in. Si carrier wafer. The walls of the chamber were held at ~150 °C to minimize reactant condensation. $SF_6$ plasma and TMA were used as the reactants. $SF_6$ plasma was struck with 30 sccm $SF_6$ and 150 sccm Ar mixing gas for 1 s and stabilized at 100 W power with 50 sccm $SF_6$ and 150 sccm Ar mixing gas for 2 s. The TMA was dosed with 100 sccm Ar carrier gas for 1 s. The precursor was then held in the chamber for 20 s without flowing gas or purging. The stage temperature was set at 200, 250, and 300 °C.

## III. RESULTS AND DISCUSSION

Figure 1(b) shows the AlN film thickness change vs cycle number for different process temperatures with other parameters fixed. At 200 °C, we observe an initial etch in the first 10 cycles followed by a subsequent thickness increase, with negligible etching



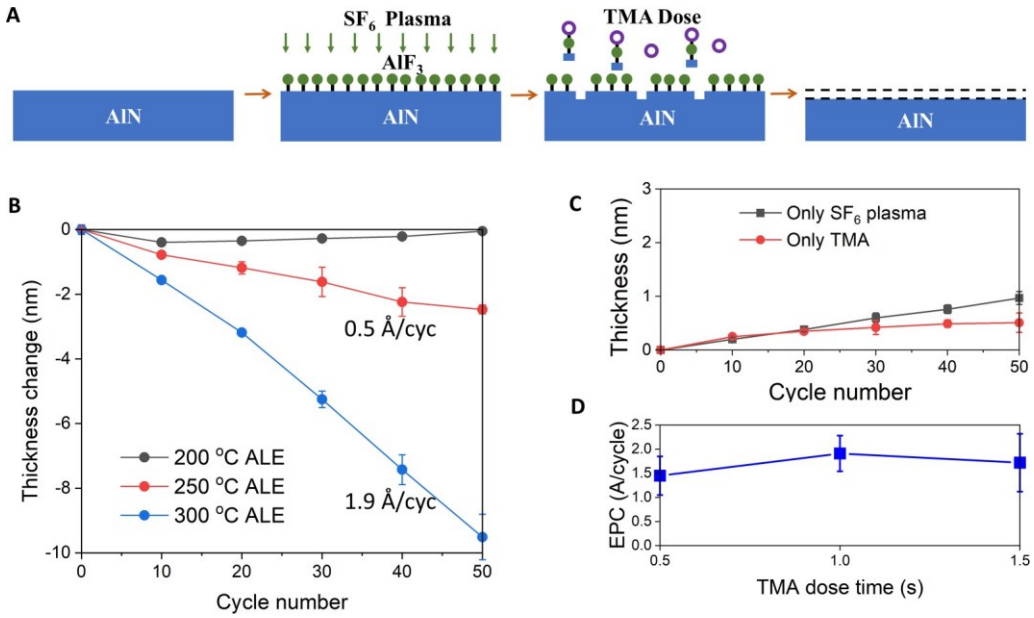


FIG. 1. (a) Isotropic plasma ALE of AlN. A low-power (100 W) $SF_6$ plasma containing F radicals (dots) is first used to fluorinate the surface. TMA (circles) is introduced to perform ligand exchange with $AlF_3$, yielding isotropic etching. (b) AlN thickness vs cycle number at different temperatures. The EPC is calculated based on the change in thickness after 50 cycles. (c) Thickness change vs cycle number for $SF_6$ plasma-only and TMA-only recipes at 300 °C, confirming that etching requires both steps of the ALE process. (d) EPC vs TMA dose time at 300 °C. Lines are guides to the eye. Error bars are as indicated or the size of the symbol.

overall after 50 cycles. At 250 °C, a monotonic trend of thickness change with cycle number is observed with an EPC of 0.5 Å/cycle. A maximum EPC of 1.9 Å/cycle is achieved at 300 °C. The EPC increase with temperature is generally consistent with prior thermal ALE studies,[25] and those using the isotropic plasma ALE approach employed here.[36] To confirm that both half-reactions are required for etching, in Fig. 1(c), we show the measured thickness change vs cycle number for $SF_6$-plasma-only and TMA-only processes at 300 °C. No etching is observed with either recipe. These results support the proposed atomic layer etching mechanism requiring both half-reactions.

We additionally examined the variation with EPC for other ALE conditions. First, we performed ALE with different TMA dose times with fixed plasma dose time at 300 °C. The results are shown in Fig. 1(d) and indicate that a dose time of 1.0 s yields the highest EPC, although the results are relatively insensitive to TMA dose time. Following a conversion-etch approach to convert the surface of aluminum nitride to alumina, we additionally attempted a three-step ($O_2$ plasma + $SF_6$ plasma + TMA dose) recipe by adding an initial 2 s oxygen plasma exposure. This recipe gave a lower EPC of 0.8 Å at 300 °C and took more time due to the additional step, and it was not investigated further.

The chemical composition of original AlN thin films was characterized by XPS. In Fig. 2, the XPS core levels for the Al2p, N1s, O1s, and F1s peaks are shown. We adopt the subpeak assignment from Ref. 48 unless specified otherwise. For the Al2p spectrum [Fig. 2(a)] of the original AlN thin film, we observe two subpeaks at 73.7 and 74.4 eV, assigned to Al−N and Al−O bonds, respectively. The O1s energy profile for AlN before ALE is shown in Fig. 2(b), and two subpeaks separated by 1.4 eV can be identified. We assign these two subpeaks to the O−Al bond in the bulk and grain boundaries, respectively. The N1s core level spectrum [Fig. 2(c)] has a primary N-Al subpeak at 396.8 eV and a secondary N-Al-O subpeak at 398.0 eV.

We performed XPS depth profiling to determine the atomic concentration in the surface and bulk. As shown in Fig. 3(a), the atomic concentrations at the surface of the original AlN film are 45.7% (Al), 27.4% (N), and 26.4% (O). Below ~4 nm (after 60 s Ar ion beam exposure), the atomic concentrations plateau to their bulk values of 55.2% (Al) 40.6% (N) 4.13% (O). The higher oxygen

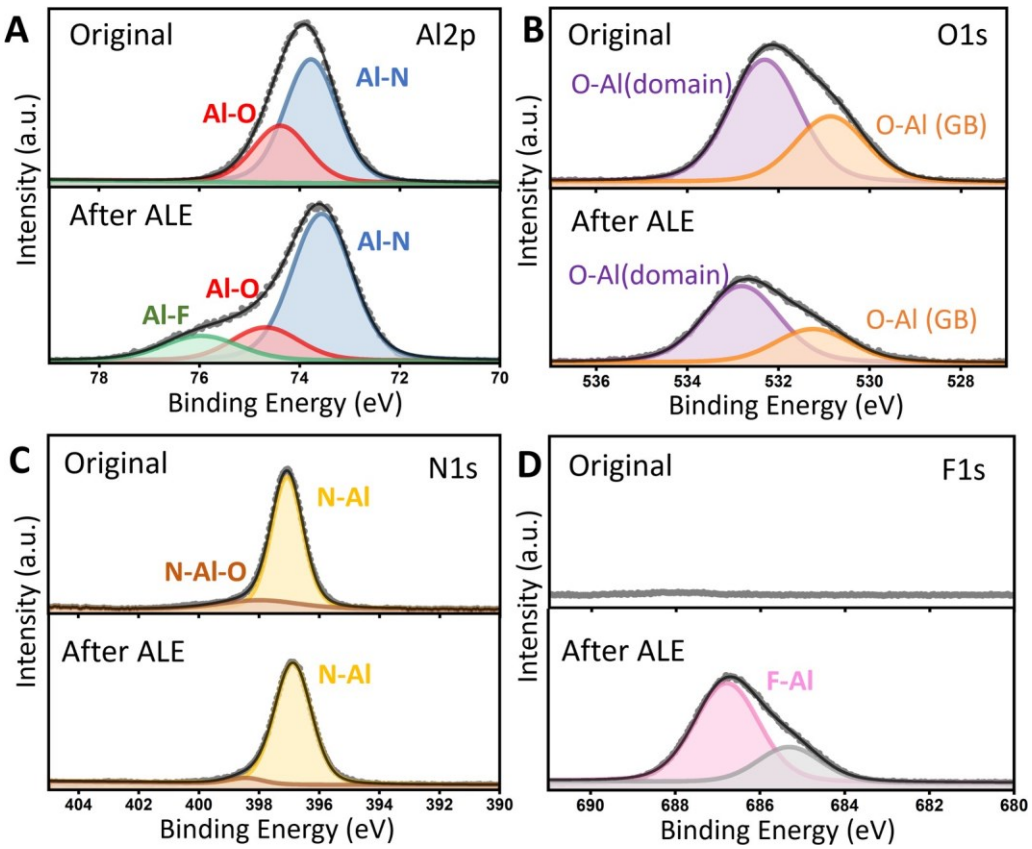


FIG. 2. AlN surface chemistry as characterized by XPS. XPS spectra of (a) Al2p, (b) O1s, (c) N1s, and (d) F1s spectra before (up) and after (down) ALE. GB, grain boundary. The measured and fit spectra are shown as the gray dots and the black line, respectively. The x axis is the binding energy, and the y axis is intensity in arbitrary units.

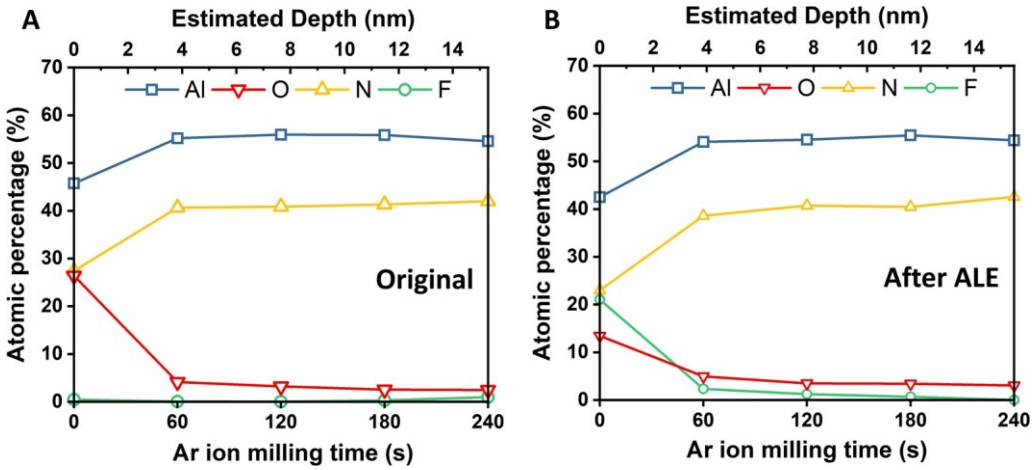


FIG. 3. Atomic concentration of Al, O, N, F vs XPS Ar ion milling time for (a) original and (b) ALE-treated AlN thin films.

concentration at the surface is consistent with the presence of a native oxide, which is known to exist in AlN films.[45,48,49]

We now examine the composition after ALE. In Fig. 2(d), we observe the appearance of an F1s peak after ALE, indicating the presence of residual fluorine in the surface. The F1s peak has primary subpeaks at 686.8 eV, assigned to Al-F, which is consistent with prior studies on fluorinated AlN.[50] Prior work also reported an additional subpeak with weaker intensity;[51–53] this subpeak is also observed here at 685.2 eV. This subpeak lacks a known assignment. For the Al2p spectrum after ALE shown in Fig. 2(a), an additional subpeak at 76.0 eV is observed and assigned to the Al−F bond.[50] The O1s energy profile after ALE is shown in Fig. 2(b) with same O-Al subpeaks for bonds in the domain and at grain boundaries. For N1s, the position of the secondary peak is shifted to 398.4 eV, but the intensity is <5% of the total N1s intensity. To the best of our knowledge, a bond assignment for this subpeak is not available.

The XPS depth profile of the ALE-treated AlN sample is shown in Fig. 3(b). It is notable that the surface oxygen concentration decreased to 13.5%, indicating a lesser presence of native oxide compared to the original film. The fluorine concentration is found to be 21% at the surface. After 60 s Ar ion milling, the fluorine concentration decreases to 2% and the fractions of Al and N are within 95% of those in the original film. This observation confirms that the alteration to the chemical composition of the film from the $SF_6$ plasma is confined to within a few nanometers of the surface without affecting the properties in the bulk, consistent with the findings of other works involving the interactions of fluorine plasmas with dielectric films.[53]

We next characterized the surface roughness of the film before and after ALE using Atomic Force Microscopy (AFM). Figures 4(a) and 4(b) show AFM images of the film before and after ALE at 300 °C, respectively. Over an area of 0:5 × 0:5 $\mu m^2$, the RMS roughness decreased ~35%, from 4.3 to 2.7 Å, after 50 cycles of ALE. The RMS roughness vs cycle number is plotted in Fig. 4(c). A monotonic decrease in surface roughness is observed with the cycle number. This observation was reproduced on three separate regions on each sample.

The PSD of the surface was computed using the measured AFM scans. The PSD provides a quantitative measure of the lateral distance over which the surface profile varies in terms of spatial frequencies.[54–57] The PSD was calculated by removing tilt via linear plane-fit and subsequently performing a 1D-discrete Fourier transform over each row and column in the raw AFM data. The transformed data were then averaged along one dimension to produce a single PSD curve. The PSD computed from Figs. 4(a) and 4(b) is plotted in Fig. 4(d). A uniform decrease in roughness is observed over a wide range of spatial frequencies, indicating that features with wavelengths from 4 to 50 nm are smoothed by the ALE process.

We now discuss the characteristics of our isotropic plasma ALE process in context with thermal ALE processes for AlN and related materials. Thermal ALE of AlN has been reported previously using HF and $Sn(acac)_2$[45] and HF or $XeF_2$ and $BCl_3$.[46] The maximum EPC reported for the latter process was 0.93 Å/cycle at a substrate temperature of 300 °C.[46] Neglecting possible differences between stage and substrate temperatures, the present process achieves a nearly twofold increase in EPC at a comparable temperature comparing with AlN ALE recipes, which do not employ plasma. The present process also enables similar EPCs as the thermal process at lower temperatures. In the former process using HF and $Sn(acac)_2$,[45] the addition of an $H_2$ plasma exposure increased the EPC to 1.96 Å/cycle, comparable to the EPC obtained here. However, the role of the plasma is different from the two processes; in Ref. 45, the plasma is used to remove $Sn(acac)_2$ residuals, while the $SF_6$ plasma here fluorinates the surface for the subsequent ligand-exchange reaction. For similar EPC values (1.9 Å/cycle), the present recipe requires two steps at 300 °C compared to three at 275 °C for that of Ref. 45.

Our isotropic plasma ALE process may find potential applications in on-chip nonlinear and quantum photonics based on AlN, for which scattering by surface imperfections represents a primary limitation for various figures of merit. Based on the measured PSD, our process decreases surface roughness of

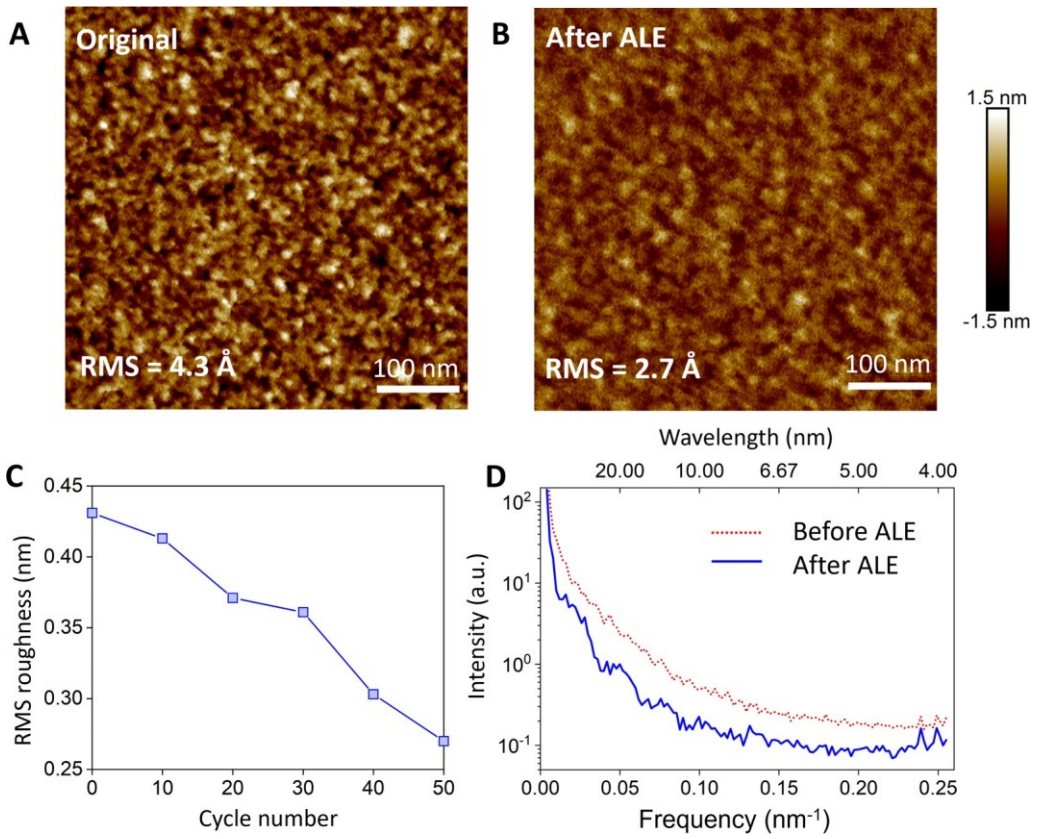


FIG. 4. Smoothing effect of isotropic plasma ALE. An AFM image of (a) the original surface and (b) after 50 cycles of ALE at 300 °C. The root mean square (RMS) roughness is calculated and labeled in the images. (c) Surface roughness vs ALE cycle number, indicating a monotonic decrease in roughness with the cycle number. Lines are guides to the eye. (d) Surface power spectral density (PSD) (arbitrary units) vs spatial frequency (bottom axis) and wavelength (top axis) for the original sample (red dotted line) and the etched sample (blue solid line). ALE uniformly decreases surface roughness over a range of spatial frequencies.



features with wavelengths up to tens of nanometers. This smoothing capability may enable the reduction in sidewall roughness due to reactive ion etching as well as lithographic roughness transferred from the resist to the film, which would in turn reduce optical losses. The ALD system in our work (Oxford Instruments, FlexAl) has demonstrated high uniformity on 200 mm diameter substrates,[58] and our recipe, therefore, has potential to extend to wafer-scale applications. Another topic worthy of investigation is the ALE of AlN prepared by different synthesis methods, such as chemical vapor deposition, as the etch characteristics of ALE are affected by sample crystallinity or other properties.[59]

## IV. SUMMARY AND CONCLUSIONS

In summary, we reported an isotropic plasma ALE process for AlN using sequential $SF_6$ plasma and $Al(CH_3)_3$ exposures. The etch rate reaches a maximum of 1.9 Å/cycle at 300 °C. We observe a smoothing effect from ALE, with a decrease in the RMS roughness of ~35% after 50 cycles. The surface oxygen content is significantly decreased after ALE, indicating that native oxides are largely removed by the process. We anticipate that the ability to engineer the surface of AlN films on the subnanometer scale using isotropic plasma ALE will facilitate applications of AlN in nonlinear photonics and electronics.

## ACKNOWLEDGMENTS

This work was supported by the Kavli Foundation and by the AFOSR under Grant No. FA9550-19-1-0321. The authors thank Nicholas Chittock, Guy DeRose, Harm Knoops, Kelly McKenzie, and Russ Renzas for useful discussions. We gratefully acknowledge the critical support and infrastructure provided for this work by The Kavli Nanoscience Institute and the Molecular Materials Research Center of the Beckman Institute at the California Institute of Technology.

## AUTHOR DECLARATIONS

### Conflict of Interest

The authors have no conflicts to disclose.

## Author Contributions

Haozhe Wang: Conceptualization (equal); Data curation (equal); Formal analysis (equal); Investigation (equal); Methodology (equal); Supervision (equal); Validation (equal); Writing – original draft (equal); Writing – review & editing (equal). Azmain Hossain: Data curation (supporting); Formal analysis (supporting); Investigation (supporting). David Catherall: Data curation (supporting); Formal analysis (supporting); Investigation (supporting); Methodology (supporting). Austin J. Minnich: Conceptualization (equal); Formal analysis (equal); Funding acquisition (equal); Investigation (equal); Methodology (equal); Project administration (equal); Resources (equal); Supervision (equal); Validation (equal); Visualization (equal); Writing – original draft (equal); Writing – review & editing (equal).

## DATA AVAILABILITY

The data that support the findings of this study are available from the corresponding author upon reasonable request.

## REFERENCES

[1]C. Xiong, W. H. Pernice, X. Sun, C. Schuck, K. Y. Fong, and H. X. Tang, New J. Phys. 14, 095014 (2012).
[2]T.-J. Lu *et al.*, Opt. Express 26, 11147 (2018).
[3]B. Dong *et al.*, Opt. Lett. 44, 73 (2019).
[4]P. T. Lin, H. Jung, L. C. Kimerling, A. Agarwal, and H. X. Tang, Laser Photonics Rev. 8, L23 (2014).
[5]Y. Taniyasu, M. Kasu, and T. Makimoto, Nature 441, 325 (2006).
[6]S. Zhao *et al.*, Sci. Rep. 5, 1 (2015).
[7]H.-S. Jang *et al.*, preprint arXiv:2208.01377 (2022).
[8]N. H. Wan *et al.*, Nature 583, 226 (2020).
[9]W. H. P. Pernice, C. Xiong, C. Schuck, and H. Tang, Appl. Phys. Lett. 100, 091105 (2012).
[10]Y. Sun, W. Shin, D. A. Laleyan, P. Wang, A. Pandey, X. Liu, Y. Wu, M. Soltani, and Z. Mi, Opt. Lett. 44, 5679 (2019).
[11]X. Liu, Z. Gong, A. W. Bruch, J. B. Surya, J. Lu, and H. X. Tang, Nat. Commun. 12, 1 (2021).
[12]W. H. P. Pernice, C. Xiong, C. Schuck, and H. Tang, Appl. Phys. Lett. 100, 223501 (2012).
[13]D. D. Hickstein *et al.*, Phys. Rev. Appl. 8, 014025 (2017).
[14]H. Oikawa *et al.*, Thin Solid Films 574, 110 (2015).
[15]C.-M. Zetterling, M. Östling, C. I. Harris, N. Nordell, K. Wongchotigul, and M. G. Spencer, *Materials Science Forum*, Stockholm, Sweden, 31 August–5 September (Trans Tech Publications, Inc., Stafa-Zurich, Switzerland, 1998), Vol. 264, pp. 877–880.
[16]Y. J. Lee, J. Cryst. Growth 266, 568 (2004).
[17]T. Adam, J. Kolodzey, C. Swann, M. Tsao, and J. Rabolt, Appl. Surf. Sci. 175, 428 (2001).
[18]H.-W. Zan, K.-H. Yen, C.-H. Chen, P.-K. Liu, K.-H. Ku, and J. Hwang, Electrochem. Solid-State Lett. 10, H8 (2006).
[19]M. De Souza, S. Jejurikar, and K. Adhi, Appl. Phys. Lett. 92, 093509 (2008).
[20]C. Besleaga, G. Stan, I. Pintilie, P. Barquinha, E. Fortunato, and R. Martins, Appl. Surf. Sci. 379, 270 (2016).
[21]D. Buttari *et al.*, Appl. Phys. Lett. 83, 4779 (2003).
[22]H. Chen, ACS Photonics 8, 1344 (2021).
[23]I. Krasnokutska, J.-L. J. Tambasco, X. Li, and A. Peruzzo, Opt. Express 26, 897 (2018).
[24]K. J. Kanarik, T. Lill, E. A. Hudson, S. Sriraman, S. Tan, J. Marks, V. Vahedi, and R. A. Gottscho, J. Vac. Sci. Technol. A 33, 020802 (2015).
[25]S. M. George, Acc. Chem. Res. 53, 1151 (2020).
[26]X. Sang, Y. Xia, P. Sautet, and J. P. Chang, J. Vac. Sci. Technol. A 38, 043005 (2020).
[27]H. C. Knoops, T. Faraz, K. Arts, and W. M. Kessels, J. Vac. Sci. Technol. A 37, 030902 (2019).
[28]M. N. Yoder, "Atomic layer etching," Technical Report, Department of the Navy, Washington, DC, 1988.
[29]H. Sakaue, S. Iseda, K. Asami, J. Yamamoto, M. Hirose, and Y. Horiike, Jpn. J. Appl. Phys. 29, 2648 (1990).
[30]Y. Horiike, T. Tanaka, M. Nakano, S. Iseda, H. Sakaue, A. Nagata, H. Shindo, S. Miyazaki, and M. Hirose, J. Vac. Sci. Technol. A 8, 1844 (1990).
[31]Y. Lee, C. Huffman, and S. M. George, Chem. Mater. 28, 7657 (2016).
[32]J. W. DuMont and S. M. George, J. Chem. Phys. 146, 052819 (2017).
[33]J. Hennessy, C. S. Moore, K. Balasubramanian, A. D. Jewell, K. France, and S. Nikzad, J. Vac. Sci. Technol. A 35, 041512 (2017).
[34]D. R. Zywotko, J. Faguet, and S. M. George, J. Vac. Sci. Technol. A 36, 061508 (2018).
[35]A. M. Cano, A. E. Marquardt, J. W. DuMont, and S. M. George, J. Phys. Chem. C 123, 10346 (2019).
[36]N. J. Chittock, M. F. Vos, T. Faraz, W. M. Kessels, H. C. Knoops, and A. J. Mackus, Appl. Phys. Lett. 117, 162107 (2020).
[37]R. Rahman, E. C. Mattson, J. P. Klesko, A. Dangerfield, S. Rivillon-Amy, D. C. Smith, D. Hausmann, and Y. J. Chabal, ACS Appl. Mater. Interfaces 10, 31784 (2018).
[38]J. W. DuMont, A. E. Marquardt, A. M. Cano, and S. M. George, ACS Appl. Mater. Interfaces 9, 10296 (2017).
[39]W. Lu, Y. Lee, J. C. Gertsch, J. A. Murdzek, A. S. Cavanagh, L. Kong, J. A. Del Alamo, and S. M. George, Nano Lett. 19, 5159 (2019).
[40]A. Fischer, A. Routzahn, S. M. George, and T. Lill, J. Vac. Sci. Technol. A 39, 030801 (2021).
[41]C. Fang, Y. Cao, D. Wu, and A. Li, Prog. Nat. Sci.: Mater. Int. 28, 667 (2018).
[42]Y. Lee, J. W. DuMont, and S. M. George, ECS J. Solid State Sci. Technol. 4, N5013 (2015).
[43]K. J. Kanarik *et al.*, J. Vac. Sci. Technol. A 35, 05C302 (2017).
[44]T. Ohba, W. Yang, S. Tan, K. J. Kanarik, and K. Nojiri, Jpn. J. Appl. Phys. 56, 06HB06 (2017).
[45]N. R. Johnson, H. Sun, K. Sharma, and S. M. George, J. Vac. Sci. Technol. A 34, 050603 (2016).
[46]A. M. Cano, A. Lii-Rosales, and S. M. George, J. Phys. Chem. C 126, 6990 (2022).
[47]J. W. Clancey, A. S. Cavanagh, J. E. Smith, S. Sharma, and S. M. George, J. Phys. Chem. C 124, 287 (2019).
[48]L. Rosenberger, R. Baird, E. McCullen, G. Auner, and G. Shreve, Surf. Interface Anal. 40, 1254 (2008).
[49]P. Motamedi and K. Cadien, Appl. Surf. Sci. 315, 104 (2014).
[50]M. Watanabe, Y. Mori, T. Ishikawa, H. Sakai, T. Iida, K. Akiyama, S. Narita, K. Sawabe, and K. Shobatake, J. Vac. Sci. Technol. A 23, 1647 (2005).
[51]J. Hennessy, A. D. Jewell, K. Balasubramanian, and S. Nikzad, J. Vac. Sci. Technol. A 34, 01A120 (2016).
[52]J. C. Moreno-López, G. Ruano, J. Ferrón, P. Ayala, and M. C. Passeggi, Jr., Phys. Status Solidi B 255, 1800389 (2018).
[53]A. Fischer, R. Janek, J. Boniface, T. Lill, K. Kanarik, Y. Pan, V. Vahedi, and R. A. Gottscho, Proc. SPIE 10149, 101490H (2017).
[54]J. M. Elson and J. M. Bennett, Appl. Opt. 34, 201 (1995).
[55]T. J. Myers, J. A. Throckmorton, R. A. Borrelli, M. O'Sullivan, T. Hatwar, and S. M. George, Appl. Surf. Sci. 569, 150878 (2021).
[56]P. Dash *et al.*, Appl. Surf. Sci. 256, 558 (2009).
[57]Y. Gong, S. T. Misture, P. Gao, and N. P. Mellott, J. Phys. Chem. C 120, 22358 (2016).
[58]J. Van Hemmen, S. Heil, J. Klootwijk, F. Roozeboom, C. Hodson, M. Van de Sanden, and W. Kessels, J. Electrochem. Soc. 154, G165 (2007).
[59]J. A. Murdzek, A. Rajashekhar, R. S. Makala, and S. M. George, J. Vac. Sci. Technol. A 39, 042602 (2021).